# Simultaneous DNA Binding and Bending by EcoRV Endonuclease Observed by Real-Time Fluorescence†

David A. Hiller,‡ Jonathan M. Fogg,‡ Amy M. Martin, Joseph M. Beechem,§ Norbert O. Reich, and John J. Perona*

*Department of Chemistry and Biochemistry and Interdepartmental Program in Biomolecular Science and Engineering, University of California at Santa Barbara, Santa Barbara, California 93106-9510*

*Received August 25, 2003; Revised Manuscript Received October 15, 2003*

ABSTRACT: The complete catalytic cycle of EcoRV endonuclease has been observed by combining fluorescence anisotropy with fluorescence resonance energy transfer (FRET) measurements. Binding, bending, and cleavage of substrate oligonucleotides were monitored in real time by rhodamine-x anisotropy and by FRET between rhodamine and fluorescein dyes attached to opposite ends of a 14-mer DNA duplex. For the cognate GATATC site binding and bending are found to be nearly simultaneous, with association and bending rate constants of $(1.45-1.6) \times 10^8$ $M^{-1}$ $s^{-1}$. On the basis of the measurement of $k_{off}$ by a substrate-trapping approach, the equilibrium dissociation constant of the enzyme−DNA complex in the presence of inhibitory calcium ions was calculated as $3.7 \times 10^{-12}$ M from the kinetic constants. Further, the entire DNA cleavage reaction can be observed in the presence of catalytic $Mg^{2+}$ ions. These measurements reveal that the binding and bending steps occur at equivalent rates in the presence of either $Mg^{2+}$ or $Ca^{2+}$, while a slow decrease in fluorescence intensity following bending corresponds to $k_{cat}$, which is limited by the cleavage and product dissociation steps. Measurement of $k_{on}$ and $k_{off}$ in the absence of divalent metals shows that the DNA binding affinity is decreased by 5000-fold to $1.4 \times 10^{-8}$ M, and no bending could be detected in this case. Together with crystallographic studies, these data suggest a model for the induced-fit conformational change in which the role of divalent metal ions is to stabilize the sharply bent DNA in an orientation suitable for accessing the catalytic transition state.

Enzyme−nucleic acid complexes often undergo significant rearrangement prior to attaining the specific conformation required to initiate catalysis. Although this induced-fit process necessarily incurs an entropic penalty relative to preformed and rigid macromolecular partners, the built-in flexibility may nonetheless increase the kinetic association rate, thus lowering the free energy barrier for complex formation (*1*). Induced fit in enzymes also represents an underlying mechanism capable of providing substrate specificity (*2*). For example, binding of a nucleic acid-modifying enzyme to a noncognate sequence may generate a different set of conformational changes than is brought about in the specific complex (*3*). As a consequence, the catalytic groups of noncognate substrates in the final quaternary complex could be misaligned with respect to each other, resulting in decreased rates for the chemical steps of the reaction.

Restriction endonucleases have provided outstanding model systems to explore the role of induced fit in generating specificity for their target sequences. In vivo, these homodimeric enzymes are capable of selecting their dyad-symmetric cognate sites despite the presence of an enormous molar excess of nonspecific DNA, with specificities of at least $10^6$-fold in $k_{cat}/K_m$ (*4*, *5*). Crystallographic studies have offered much insight into both the conformational differences among specific, noncognate, and nonspecific complexes (*6*, *7*) and the structural pathway by which the specific complex is attained (*8*). However, understanding the mechanistic importance of these conformational changes also requires determination of the temporal correlation between the initial binding of the restriction enzyme to the DNA and the subsequent rearrangements en route to the transition state.

A further important feature of the conformational rearrangements is that they bring about the formation of divalent metal binding sites at the interface between the enzyme and DNA. For example, in EcoRV endonuclease four distinct metal sites per subunit have been located at the DNA interface, three of which are directly adjacent to the scissile phosphate (*9*−*11*). Divalent metals ($Mg^{2+}$, $Mn^{2+}$, or $Co^{2+}$) are required to generate high binding affinity, to provide for much of the sequence specificity of binding, and to promote the phosphoryl transfer reaction (*12*−*19*). $Ca^{2+}$ allows EcoRV binding to DNA with high specificity but blocks the cleavage reaction (*14*, *18*, *19*). This ion is thus a useful analogue to isolate the binding and conformational change steps of the pathway and to trap the complex prior to cleavage for X-ray studies (*20*). High-resolution structures of the trapped complex reveal that EcoRV bends the DNA sharply by 50° at the center TA step of the GATATC target sequence, opening up the minor groove for protein interaction and formation of the metal sites for blunt-ended cleavage at 5′-TpA-3′.

Rapid reaction analysis of the EcoRV catalytic cycle has previously been performed by monitoring the intrinsic tryptophan fluorescence of the protein (*15*, *17*). Although hampered by a low signal to noise ratio, these experiments

† This work was supported by National Science Foundation Grant MCB-9983125 (to N.O.R.) and National Institutes of Health Grant GM53763 (to J.J.P.).

* To whom correspondence should be addressed. Telephone: (805) 893-7389. Fax: (805) 893-4120. E-mail: perona@chem.ucsb.edu.

‡ These authors contributed equally to this work.

§ Present address: Molecular Probes, Inc., Eugene, OR 97402.

10.1021/bi035520w CCC: $25.00 
Published on Web 11/20/2003

nonetheless showed an initial very rapid fluorescence increase of approximately 200 $s^{-1}$ attributable to binding, followed by a slow decrease on the order of the reaction steady-state $k_{cat}$ (0.2 $s^{-1}$), corresponding to DNA cleavage and product release. Fluorescence anisotropy and fluorescence resonance energy transfer (FRET)[1] studies on EcoRV have also been performed using DNA singly end-labeled with a fluorescent probe (*21*, *22*). These experiments provided further evidence that specific binding to DNA is highly dependent upon divalent metal ions.

In this work, we sought to further expand the use of fluorescence techniques as applied to EcoRV by developing new approaches to characterize the DNA bending and concomitant induced-fit transitions. Stopped-flow anisotropy measurements using an enhanced light source and rhodamine-x- (RhX-) labeled duplex oligonucleotide substrates were used to determine the on and off rates for DNA binding, thereby yielding the equilibrium $K_d$ via the ratio of the rate constants. In this manner thermodynamic equilibrium constants can be calculated directly from the kinetic data, allowing determination of picomolar DNA-binding affinities in solution. This approach provides an alternative to the laborious and often ambiguous equilibrium measurements performed via gel shift or filter binding techniques, each of which are prone to artifacts arising from macromolecular interactions with the physical matrix. Separately, stopped-flow FRET was carried out using an optimized doubly labeled DNA substrate in which fluorescein (Fl) and rhodamine (Rh) were employed as the donor and acceptor fluorophores, respectively. In contrast to previous EcoRV fluorescence studies which provided only a general binding signal, these FRET experiments now allow for direct monitoring of the DNA bending rate. By these approaches we have determined that for specific sites the rate of DNA binding is essentially synchronous with the rate of bending; thus, these two processes occur in a single effectively concerted step. Interestingly, while the association rate is very high in the absence of metal ions, no DNA bending can be detected in this case. Together with the detailed structural descriptions available in multiple conformational states, these kinetic methods open new possibilities for characterizing the induced-fit pathway of this enzyme−nucleic acid complex at an extremely detailed level. This may be ultimately crucial for our ability to rationally manipulate the specificities of EcoRV and other restriction endonucleases.

## MATERIALS AND METHODS

*Enzyme Purification.* EcoRV endonuclease was overexpressed from the plasmid pBSRV in *Escherichia coli* strain MM294 and purified to better than 99% homogeneity by column chromatography, as previously described (*20*, *23*−*25*). Enzyme preparations were dialyzed into 10% (v/v) glycerol, 0.4 M NaCl, 20 mM potassium phosphate (pH 7.3), and 1 mM dithiothreitol and were concentrated to 2.6 mg $mL^{-1}$ [$\epsilon$ = 1.8 mL (mg cm)$^{-1}$ at 280 nm]. Aliquots were flash-frozen and stored at −70 °C. Alternatively, enzyme was stored at 5.9 mg $mL^{-1}$ at −20 °C following dialysis into 50% (v/v) glycerol, 0.2 M NaCl, 20 mM potassium phosphate (pH 7.3), and 10 mM $\beta$-mercaptoethanol. The two preparations gave identical results.

*DNA Synthesis and Dye Coupling.* DNA oligonucleotides were synthesized at the UCSF Biomolecular Resources Center and by Integrated DNA Technologies, Inc. (IDT). 5- (and 6-) Carboxyfluorescein succinimidyl ester (Fl), tetramethylrhodamine 5- (and 6-) isothiocyanate (Rh), and rhodamine-x 5- (and 6-) isothiocyanate (RhX) were purchased from Molecular Probes, Inc. Oligonucleotides were synthesized with a primary amino group connected by a six-methylene spacer (either C6 amino linker, Glen Research No. 10-1916-02, or Amino Modifier C6, IDT). DNA was precipitated with ethanol, and the recovered pellets were resuspended at a concentration of 25 $\mu$g $\mu L^{-1}$ in 0.1 M sodium tetraborate (pH 8.5). Fl and either Rh or RhX were dissolved in DMSO to ~20 $\mu$g $\mu L^{-1}$. These dyes were added dropwise to the appropriate oligonucleotide (at 10-fold final molar dye excess), and the reactions were stirred overnight in the dark at 25 °C with gentle vortexing every half hour for the first 2 h. The reaction products were ethanol precipitated to remove excess dye. The DNA pellets were resuspended in TE buffer (10 mM Tris, 1 mM EDTA, pH 8.0), combined with an equal volume of formamide, heated for 3 min at 90 °C, and loaded onto two prerunning 20% native polyacrylamide gels (gel dimensions 31.0 cm × 38.5 cm × 1.4 mm), followed by electrophoresis for 3−5 h at 400 V. The labeled DNAs migrated as visible bands and were run near to the bottom of the gel. Unlabeled DNA was visualized by UV shadowing and ran as a discrete band below the labeled DNA. The labeled DNA was eluted into TE buffer from gel slices overnight in the dark. The eluted DNA was reprecipitated with ethanol and resuspended in TE buffer.

DNA concentrations were determined spectrophotometrically at 260 nm with extinction coefficients calculated using software based upon the reported pairwise extinction data. To verify complete labeling, Rh, RhX, and Fl concentrations were also determined spectrophotometrically for the labeled DNA at the following wavelengths: Rh, 555 nm; RhX, 585 nm; Fl, 494 nm. These concentrations were compared to those determined at 260 nm, and the DNA substrates were thus found to be ≥90% labeled. Complementary strands were annealed at an equimolar ratio in a buffer containing 10 mM Tris (pH 8.0), 1 mM EDTA, and 100 mM NaCl by heating to 90 °C for 10 min followed by a slow decrease to 25 °C over at least 3 h.

The DNA sequences used were as follows: Fl-TAtop, Fl-d(AGAAGATATCTTGA); Fl-GCtop, Fl-d(GGCGGATATCGCGG); Rh-TAbot, Rh-d(TCAAGATATCTTCT); RhX-GCbot, RhX-d(CCGCGATATCCGCC); GCtop, d(GGCGGATATCGCGG); TAbot, d(TCAAGATATCTTCT); GCbot, d(CCGCGATATCCGCC). The designations "GC" and "TA" refer to the identity of the terminal base pair. Binding studies by fluorescence anisotropy utilized duplexes Fl-GCtop/GCbot and GCtop/RhX-GCbot. Studies of bending rates by FRET utilized duplexes Fl-TAtop/Rh-TAbot or Fl-GCtop/RhX-GCbot; these two duplex substrates, which differ in the sequence flanking the target site, gave identical rates.

*Fluorescence Anisotropy.* Steady-state measurements were collected on a SPEX 1681 Fluorolog spectrofluorometer (Edison, NJ) at 24 °C. RhX anisotropy was determined by collecting emission spectra with $\lambda_{ex}$ = 580 nm. $\lambda_{em}$ was

[1] Abbreviations: Fl, 5- (and 6-) carboxyfluorescein succinimidyl ester; RhX, rhodamine-x 5- (and 6-) isothiocyanate; Rh, tetramethylrhodamine 5- (and 6-) isothiocyanate; DMSO, dimethyl sulfoxide; FRET, fluorescence resonance energy transfer.

collected from 585 to 700 nm through vertical and horizontal polarization filters in the two detection monochromators. The excitation and emission bandwidths were 5 nm for all of the spectra. Slit widths were 2 mm/2 mm for excitation/emission unless otherwise specified. The anisotropy at $t = 0$ was determined by monitoring the duplex GCtop/RhX-GCbot for at least 30 s. Protein was then added, and the anisotropy was monitored over time at 615 nm. For measurements of $k_{off}$ in the steady-state instrument, Fl-labeled DNA was excited at 460 nm, emission was measured at 520 nm in a time-based scan with a measurement made every 0.5 s, and slit widths were decreased to 1 mm/1 mm. EcoRV (110 nM) and Fl-GCtop/GCbot (100 nM) were preequilibrated, the unlabeled competitor DNA GCtop/GCbot (1 $\mu$M) was added at $t = 0$, and the reaction was monitored over time until the anisotropy reached the free DNA value.

Stopped-flow anisotropy measurements were performed with an SFM-3 stopped-flow unit containing three independent stepper-motor driven syringes (Molecular Kinetics, Pullman, WA) with an FC.15 cuvette (50 $\mu$L volume) and a hard stop shutter. Fluorescence detection utilized a home-built single photon detector unit consisting of the following: a Hamamatsu R928 photomultiplier, a 5 × 300 MHz amplifier (Stanford Research SR445, Sunnyvale, CA), a discriminator (Stanford Research SR400), and two multichannel scaler cards (Tennelec Model MCS-II, Oak Ridge, TN), interfaced to two microcomputers (Intel 486). The detection system was activated by an external synch-out pulse from a Molecular Kinetics stepper-motor controlling unit. Data acquisition began at least 100 ms before sample mixing. Data were collected using 1−15 ms dwell times in 8000 total channels. A 250 W xenon arc lamp (SPEX Fluorolog Model 1681) with fiber-optic output directed into the 50 $\mu$L cell was used for excitation at various wavelengths. A T-format anisotropy detection scheme was used with $\lambda_{ex} = 580$ nm, and $\lambda_{em}$ was collected through 610 nm cutoff filters. The data from 15 to 20 anisotropy time courses was summed to achieve an adequate signal to noise ratio.

*Steady-State FRET Experiments.* Steady-state emission scans were made on a Perkin-Elmer luminescence spectrometer (LS50B) at 22 °C. To excite the donor (fluorescein), $\lambda_{ex}$ was set to 485 nm, and $\lambda_{em}$ was collected from 500 to 650 nm. To directly excite the acceptor (rhodamine), $\lambda_{ex}$ was moved to 555 nm, and $\lambda_{em}$ was collected from 570 to 650 nm. The excitation slit width was 8 mm, and the emission slit width was 10 mm for all of the spectra. Energy transfer was computed from the increase in acceptor fluorescence. A normalized scan of Fl-TAtop/TAbot was subtracted from the donor-excited scan to isolate the rhodamine emission. The area under this corrected scan from 575 to 585 nm divided by the area under the directly excited scan from 575 to 585 nm gave the value $\text{ratio}_A$. For the materials utilized in this study, a method which best compensates for uncertainties in the degree of labeling of the acceptor, quantum yield of the acceptor, and concentration of the DNA is a calculated FRET efficiency using the equation:

$$E = [\epsilon^A(555)/\epsilon^D(485)][\text{ratio}_A - \epsilon^A(485)/\epsilon^A(555)] \quad (1)$$

where $\epsilon^D(\lambda)$ and $\epsilon^A(\lambda)$ are the extinction coefficients at wavelength $\lambda$ of the donor and acceptor, respectively (*26*). Calculation of FRET efficiencies from the ratio of donor fluorescence intensities yielded equivalent results.

For steady-state titrations, scans of 20 nM DNA were repeated until consecutive scans were equivalent. Then aliquots of enzyme were added and allowed to equilibrate for at least 30 s. Scans of donor and acceptor excitation were taken, and the process was repeated until the signal is saturated. Plots of energy transfer as determined above against enzyme concentration were then fit to a quadratic binding equation:

$$F = \Delta F[(f^*E_0 + S_0 + K_d) - ((f^*E_0 + S_0 + K_d)^2 - 4f^*E_0S_0)^{1/2}]/2S_0 + F_0 \quad (2)$$

where $S_0$ is the original DNA concentration, $K_d$ is the equilibrium dissociation constant, $F_0$ is the energy transfer for unbound DNA, and $\Delta F$ is the total change in energy transfer upon complete binding. The factor $f$ accounts for the actual concentration of active enzyme ($f^*E_0$) being different from that determined from absorbance ($E_0$). This equation is derived directly from the expression for the equilibrium dissociation constant and from conservation of mass with no assumptions.

*Stopped-Flow FRET Experiments.* Experiments were performed using the apparatus described above for the anisotropy measurements. A T-format detection scheme was used with the polarizers removed. $\lambda_{ex} = 485$ nm, and $\lambda_{em}$ was collected through a 515 nm cutoff filter (to measure the fluorescein emission) from one detection channel and through a 610 nm cutoff filter (to measure rhodamine-x emission) from the other detection channel. The data from 4 to 15 FRET time courses were summed to achieve an adequate signal to noise ratio. Dead time values were calibrated as described (*27*). Energy transfer was measured both as the quench in donor emission (energy transfer) and as the increase in acceptor emission (sensitized acceptor). The sensitized acceptor data were corrected for variations in the total intensity of RhX emission by normalizing both the sensitized acceptor data and the total intensity data and then dividing the sensitized acceptor data by the total intensity data. Plots of the total intensity data for all reactions showed only minor variations which had virtually no effect on the sensitized acceptor data.

Stopped-flow FRET experiments yielding identical rate constants were also performed with an Applied Photophysics SX.18MV stopped-flow reaction analyzer. Energy transfer was again measured both as the quench in donor emission and as the increase in acceptor emission (through a 570 nm cutoff filter for rhodamine), though each experiment was done sequentially.

For all experiments solutions of enzyme, fluorescent-labeled DNA, and buffer alone were loaded into three separate syringes. The buffer for the $Ca^{2+}$ reactions contained 50 mM Tris (pH 7.5), 100 mM NaCl, and 10 mM $CaCl_2$. The buffer for the $Mg^{2+}$ reaction was identical to the $Ca^{2+}$ buffer except that 10 mM $MgCl_2$ replaced the $CaCl_2$. The no-metal buffer was also identical to the $Ca^{2+}$ buffer, except for inclusion of 2 mM EDTA and adjustment of the NaCl concentration to 136 mM to maintain constant ionic strength. Enzyme and DNA stocks were adjusted to the appropriate concentrations by dilution in these buffers. Reactions were initiated by mixing equal volumes (100 $\mu$L) of enzyme and DNA solutions at flow rates between 4 and 8 mL $s^{-1}$. All measurements were made at 22 °C.

*Data Analysis.* Anisotropy data for association reactions were fit to the equation:

$$A = (A_b - A_f)[1 - \Delta/([P]_0 e^{\Delta kt} - [D]_0)] + A_f \quad (3)$$

where $[P]_0$ is the initial protein concentration, $[D]_0$ is the initial DNA concentration, $k$ is the association rate constant, $t$ is the time, $A$ is the anisotropy value at time $t$, $A_f$ is the anisotropy value of unbound DNA, $A_b$ is the anisotropy value of bound DNA, and $\Delta = [P]_0 - [D]_0$. Anisotropy data for the competition experiments to determine the dissociation rate were fit to the equation:

$$A = (A_b - A_f)([P{-}D]_0 e^{-kt}) + A_f \quad (4)$$

where $[P{-}D]_0$ is the initial concentration of the protein−DNA complex and the other variables are as described above. For enzyme concentrations in excess of DNA, stopped-flow fluorescence time courses were fit to a single exponential:

$$F = (F_b - F_f)(1 - e^{-kt}) + F_f \quad (5)$$

where $F$ is the fluoresence in arbitrary units and the subscripts are as above to derive the observed rate constant. For a second-order event under these pseudo-first-order conditions, a plot of $k_{obs}$ at a variety of enzyme concentrations is linear with the slope equal to $k_{on}$ and the intercept equal to $k_{off} - k_{on}[D]_0$ (*28*). For wild-type EcoRV in the presence of calcium the $k_{on}[D]$ term dominates, and $k_{off}$ is too small to be determined by this technique. In this case, $k_{off}$ is determined by addition of excess unlabeled DNA to the prebound labeled complex, as described above.

To set limits on the relative magnitudes of the binding and bending rate constants, data were fit to the binding and bending steps of the reversible mechanism (Scheme 1) using the program Kinteksim (*29*−*31*). In the first simulations, the reverse rates of binding and bending ($k_{-1}$ and $k_{-2}$, respectively) were set to 0.001 and 0.0001 $s^{-1}$, and both forward rates $k_1$ and $k_2$ were allowed to vary. Subsequently, the forward binding rate was fixed at the value from the first simulations, and data were then simulated for several specified forward bending rates. Simulated data courses were then fit to a single exponential to determine the deviation caused by each bending rate. The later steps in the reaction pathway ($k_{chem}$, $k_3$) do not occur with $Ca^{2+}$ or in the absence of metal.

*Bend Angle Calculations.* FRET efficiency values from the titrations in the presence of calcium were used to estimate the DNA bend angle in solution. By necessity, these calculations are highly approximate. FRET efficiency was converted to distance using the Forster equation:

$$E = R_0^6/(R_0^6 + R^6) \quad (6)$$

The Forster distance, at which FRET efficiency is 0.5, is calculated from the equation (*32*):

$$R_0^6 = (8.785 \times 10^{-5})\Phi_D K^2 n^{-4} J(\nu)\ \text{Å}^6 \quad (7)$$

The overlap integral $J(\nu)$ was determined to be $2.24 \times 10^{15}$ for the fluorescein−rhodamine pair and $1.96 \times 10^{15}$ for the fluorescein−rhodamine-x pair. For both dye pairs, $\Phi_D$, $K^2$, and $n$ were estimated as 0.5, 2/3, and 1.33, respectively. The calculated Forster distances were then 52.5 Å for fluorescein−rhodamine and 51.3 Å for fluorescein−rhodamine-x.

Scheme 1: Kinetic Mechanism of EcoRV Endonuclease[a]

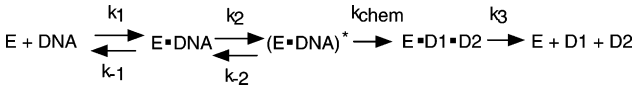


[a] (E−DNA)* represents the EcoRV complex with bent DNA, and D1 and D2 represent the two product duplexes.

The program CURVES (*33*) was applied to the cognate crystal structure to determine the direction of the bend relative to the location of the 5′-terminal phosphates. The plane in which the DNA bends was defined to be the *XZ* plane. To estimate the bend angle, the locations of the fluorophores relative to the helix ends must be estimated. Fluorescein is negatively charged and has a low anisotropy when covalently linked to DNA (*26*), implying that its preferred orientation probably avoids contact with the phosphate backbone of DNA. Therefore, fluorescein was assumed to extend out from the DNA, at an angle α with the *XY* plane. Accumulating evidence indicates that rhodamine is stacked on the DNA end (*34*, *35*) though the precise location of the fluorophore is unknown. Therefore, a variety of initial rhodamine positions were chosen. These included positions along the helix axis, above the major groove, and other positions beyond the helix end. For each assumed location, the value of α was varied until the distance between fluorophores in the absence of protein was matched. With α fixed, the bend angle was then varied until the distance in the presence of saturating protein was reached. The range of values for the bend angle with different rhodamine positions is reported. Similar methods have been used to estimate the bend angles of DNA bound to HMG1 (*36*), TBP (*37*), PAP1 (*38*), and IHF (*34*).

## RESULTS

*Steady-State Fluorescence Intensity and Resonance Energy Transfer.* Steady-state emission spectra of a 14-mer duplex DNA substrate containing the specific EcoRV site GATATC, both alone and bound to protein, are shown in Figure 1. Compared to singly Fl-labeled duplex DNA, a substantial FRET of 40% is observed in the DNA duplex doubly labeled with Fl and RhX fluorophores covalently attached at the respective 5′-termini. The strongly decreased donor emission is expected due to the strong spectral overlap of the Fl emission spectrum with the RhX excitation spectrum, which results in energy transfer from fluorescein to rhodamine-x. The Forster radius is approximately 51 Å for this dye pair, which is comparable to the expected fluorophore to fluorophore distance. Near the Forster radius energy transfer is most sensitive to changes in distances, providing a means to measure even small changes in DNA bending upon protein binding.

Binding of the singly labeled Fl-GCtop/GCbot duplex to EcoRV at saturating levels significantly increased the fluorescein emission at 520 nm (compare green and red traces, Figure 1a). For this reason, the additional energy transfer from Fl to RhX upon the addition of EcoRV to the doubly labeled Fl-GCtop/RhX-GCbot substrate is only weakly apparent from the uncorrected intensity data alone (compare black and blue traces, Figure 1a). However, the effect of protein binding on fluorescence is presumably identical on either donor-only DNA or doubly labeled DNA.

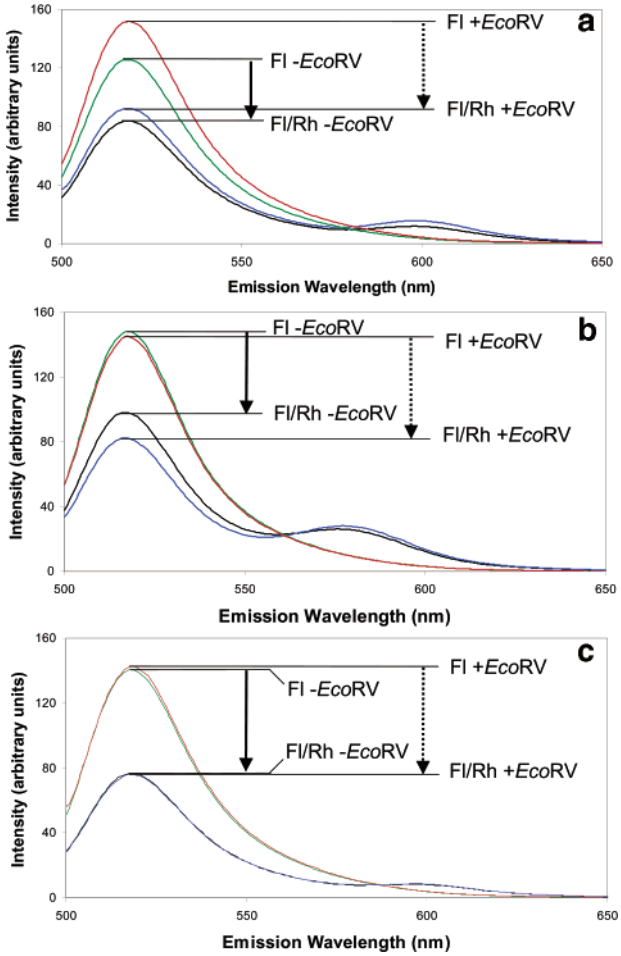


FIGURE 1: Steady-state emission scans. (a) 20 nM singly labeled substrate Fl-GCtop/GCbot in the absence (green) and presence (red) of 30 nM EcoRV and 20 nM doubly labeled substrate Fl-GCtop/RhX-GCbot in the absence (black) and presence (blue) of 30 nM EcoRV. Scans were performed in the presence of 10 mM $CaCl_2$. Direct absorption of the 485 nm excitation light gave rise to the 520 nm fluorescein emission peak; this emission was decreased by resonance energy transfer to rhodamine-x. The small shoulder at ~600 nm represents the rhodamine-x emission derived from both direct absorption of the 485 nm excitation light and the energy transfer from the donor fluorescein. The solid arrow denotes the extent to which fluorescein emission is decreased by energy transfer in the absence of protein; the dotted arrow corresponds to energy transfer in the presence of protein. The larger magnitude of the dotted arrow indicates that FRET is greater in the presence of protein, despite the apparent increase in fluorescein emission of the doubly labeled substrate. (b) Steady-state emission scans performed as in (a) for the substrates Fl-TAtop/TAbot and Fl-TAtop/Rh-TAbot. Donor emission of the singly labeled substrate does not change upon addition of enzyme, and the increase in FRET is apparent from the decrease in doubly labeled donor emission. Note that the acceptor, for this substrate, emits at ~580 nm. (c) Emission scans as in (a) but performed in the absence of divalent metal. The enzyme concentration for the red and black scans was adjusted to 200 nM to ensure that the DNA is bound.

Computation of energy transfer from the equation ET = 1 − DA/D (see Materials and Methods) corrects for this phenomenon, because the effect of protein binding is canceled out when the intensities derived from doubly and singly labeled substrates are divided. Interestingly, a second cognate sequence containing a TA instead of GC terminal base pair (Fl-TAtop/Rh-TAbot) does not show this fluorescence enhancement upon protein binding (Figure 1b). It has been reported that the quenching of fluorescein emission upon conjugation to DNA is greater for oligonucleotides containing GC versus TA terminal base pairs due to a charge transfer mechanism (*39*). Because EcoRV contacts DNA only over 10 base pairs (*7*), it is not immediately apparent how binding mitigates this effect, thereby increasing the fluorescence emission. However, charge transfer is dependent on the electron-donating ability of the oligonucleotide, indicating that indirect effects could be important. In fact, this phenomenon is not observed in the absence of divalent metal (Figure 1c), supporting the idea that the quantum yield is sensitive to subtle changes in the environment of the fluorophore. The enhanced intensity upon EcoRV binding to the GC substrate (Figure 1A) also provides another probe to investigate formation of the enzyme−substrate complex. While in this study we have chosen to examine binding affinity instead by fluorescence anisotropy (see below), preliminary results reveal that the fluorescence enhancement binding signal gives equivalent association and dissociation rates (data not shown).

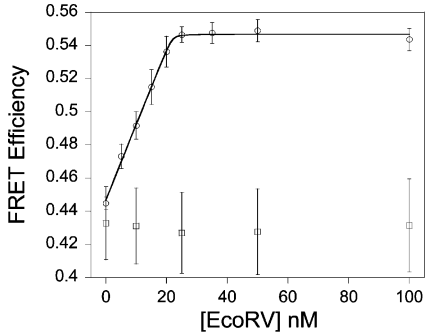


FIGURE 2: Equilibrium titrations. Energy transfer efficiency is determined from the increase in acceptor emission. 20 nM Fl-TAtop/Rh-TAbot was titrated with 5−100 nM EcoRV endonuclease in the presence (open circles) or absence (open squares) of 10 mM $CaCl_2$ at pH 7.5. Error bars correspond to two standard errors. In the presence of $Ca^{2+}$ the increase in FRET efficiency fits well to the quadratic binding equation (see Materials and Methods). The concentration of active enzyme determined from this fit is 90% of that determined by absorbance, and the $K_D$ is within experimental error of zero.

The reduced quenching of fluorescein conjugated to DNA sequences terminating with TA pairs was exploited for equilibrium FRET titrations, which utilized the dye pair Fl-TAtop/Rh-TAbot. The increased signal allows for the measurement of FRET from the acceptor emission at low DNA concentrations. These equilibrium titrations were performed in either the presence or absence of 10 mM $CaCl_2$. In both cases, 20 nM DNA was incubated with increasing concentrations of EcoRV, and the FRET efficiency was monitored through the corrected increase in rhodamine intensity. In the presence of $Ca^{2+}$ the increase fits well to the quadratic binding equation (Figure 2, open circles). The $K_D$ determined from this fit is within experimental error of zero, indicating it is too low to be obtained from this technique and instead must be determined by calculation from the kinetic constants. However, by fixing the substrate concentration the fraction of active enzyme can be left as a parameter of the fit. The active fraction of 0.90 obtained from this fit was used to correct the enzyme concentration in the experiments to follow.

The titration end points measured in the presence of $Ca^{2+}$ were used to estimate the DNA bend angle of the ternary complex. FRET efficiency values obtained from acceptor emission are less prone to error than those from donor

Table 1: DNA Binding and Bending by EcoRV Endonuclease

| conditions | $k_{on}$ ($M^{-1}$ $s^{-1}$)[a] | $k_{off}$ ($s^{-1}$)[b] | $k_{bend}$ ($M^{-1}$ $s^{-1}$)[c] | kinetic $K_d$ (M) |
|---|---|---|---|---|
| $Mg^{2+}$ | 2.2 ($\pm$0.4) $\times$ $10^8$ | | 2.0 ($\pm$0.1) $\times$ $10^8$ | |
| $Ca^{2+}$ | 1.60 ($\pm$0.01) $\times$ $10^8$ | 5.97 $\times$ $10^{-4}$ | 1.45 ($\pm$0.01) $\times$ $10^8$ | 3.7 $\times$ $10^{-12}$ |
| no metal | 1.07 ($\pm$0.02) $\times$ $10^9$ | 1.46 ($\pm$0.3) $\times$ $10^1$ | | 1.4 $\times$ $10^{-8}$ |

[a] The $k_{on}$ values were determined by fitting the association rate equation (see Materials and Methods) to the anisotropy time courses. [b] The $k_{off}$ values were determined by fitting the dissociation rate equation (see Materials and Methods) to the anisotropy time courses. $k_{off}$ could not be determined for the $Mg^{2+}$ reaction because the DNA is cleaved too rapidly. [c] The $k_{bend}$ values were determined by fitting the association rate equation to the sensitized acceptor time courses.

quenching (see Materials and Methods) and, therefore, are ideal for this calculation, which is already subject to uncertainty in the position of the fluorophores. The FRET efficiency change from 0.447 to 0.547 (Figure 2) corresponds to a change in distance from 54.6 to 50.9 Å. Depending on the assumed location of rhodamine, the calculated bend angle ranges from 30° to 65°. This estimate reasonably approximates the 50° bending angle derived from X-ray structures (*7*). More accurate determination of the DNA bending angle from FRET will require fluorescence lifetime measurements (*39*) or the use of several different helix lengths to reduce the uncertainty in the position of the fluorophores. In the absence of divalent metal (Figure 2, open squares) the FRET efficiency is unchanged even well above the $K_D$ determined under these conditions (Table 1; *18*, *19*, *21*, *22*). This indicates that the DNA is bound but not bent in the absence of divalent metal. The finding that DNA bending apparently requires metal ions was investigated further by stopped flow (see below).

*Association and Dissociation Rates by Fluorescence Anisotropy.* Fluorescence anisotropy provides a highly sensitive continuous solution-based assay for both equilibrium and kinetic measurements of protein−DNA binding. The basis for this approach is that the protein−DNA complex tumbles more slowly in solution than does the unliganded DNA, producing an increase in the anisotropy value. Although equilibrium fluorescence anisotropy experiments are typically limited to DNA concentrations in the micromolar to nanomolar range, much tighter binding constants can be derived by measuring the kinetic on and off rates using stopped-flow instrumentation. Further, while the 20% increase in total fluorescence intensity upon EcoRV binding (Figure 1) might somewhat compromise the precision of equilibrium anisotropy measurements (*21*), it should have no effect on the determinations of $k_{on}$ and $k_{off}$.

Association and dissociation rates were monitored in both the presence and absence of 10 mM $CaCl_2$. EcoRV (20 nM) and 20 nM RhX-labeled DNA were rapidly mixed in the stopped-flow instrument, and the anisotropy was monitored over time (Figure 3a). The high signal to noise stopped-flow anisotropy data sets allow a very accurate estimation of the on rate (Table 1). Interestingly, the association rate in the absence of metal ions is approximately $10^9$ $M^{-1}$ $s^{-1}$, about 8-fold faster than in the presence of either $Ca^{2+}$ or $Mg^{2+}$ (Table 1). Indeed, the rate of complex formation in the absence of $Ca^{2+}$ or $Mg^{2+}$ is so fast that most of the initial reaction occurred within the roughly 5 ms dead time of the experiment. Thus, this on rate estimate is subject to some increased uncertainty.

To determine dissociation kinetics, 110 nM EcoRV endonuclease was prebound to 100 nM fluorescein-labeled DNA. The prebound complex was then mixed with 1 $\mu$M unlabeled (i.e., nonfluorescent) 14-mer duplex DNA, and the decrease in anisotropy was monitored over time (Figure 3b). This concentration of unlabeled DNA traps 90% of the enzyme after release of the labeled substrate, sufficient to allow determination of the dissociation rate. In these experiments the anisotropy **r** decreased from 0.093 for the enzyme−DNA complex to the uncomplexed DNA value of 0.064. The dissociation rate in the presence of $Ca^{2+}$ was slow enough to allow mixing by hand in the steady-state spectrofluorometer, while the measurement in the absence of metal ions required use of the stopped-flow instrument. Upon addition of competitor in the presence of metal ions, the anisotropy drops sharply during the first few seconds of the experiment (Figure 3b). This may be indicative of a more complex, biphasic dissociation process. These data reveal that the presence of $Ca^{2+}$ causes a decrease in the DNA dissociation rate by greater than $10^4$-fold (Table 1).

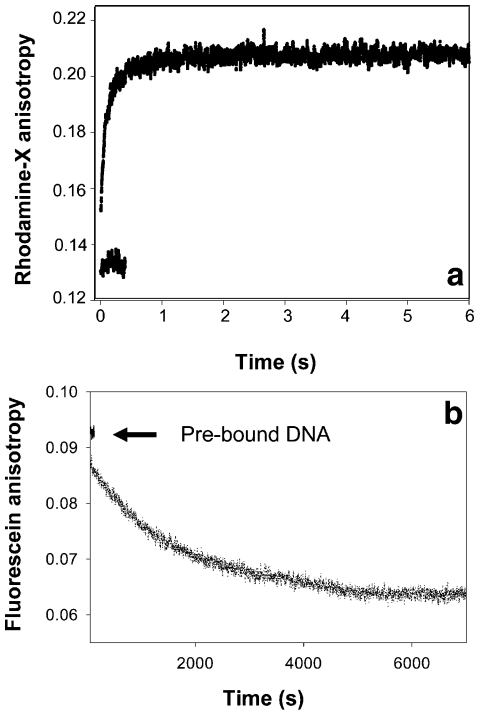


FIGURE 3: Stopped-flow anisotropy measurements. (a) Time course for determination of the association rate constant $k_{on}$. 20 nM EcoRV endonuclease was mixed with 20 nM RhX-labeled DNA (GCtop/RhX-GCbot) in the presence of 10 mM $CaCl_2$. The anisotropy of the uncomplexed DNA is also indicated. (b) Time course for determination of the dissociation rate constant $k_{off}$. 110 nM EcoRV endonuclease was premixed with 100 nM fluorescein-labeled DNA (Fl-GCtop/GCbot) in the presence of 10 mM $CaCl_2$, and the anisotropy was followed over time after addition of 1 $\mu$M unlabeled 14-mer duplex DNA.

The ratio of rate constants $k_{off}/k_{on}$ is equal to the equilibrium dissociation constant $K_d$. This value is determined as 3.7 pM in the presence of $Ca^{2+}$ and 14 nM in its absence, a difference of about 3800-fold. This level of improved affinity

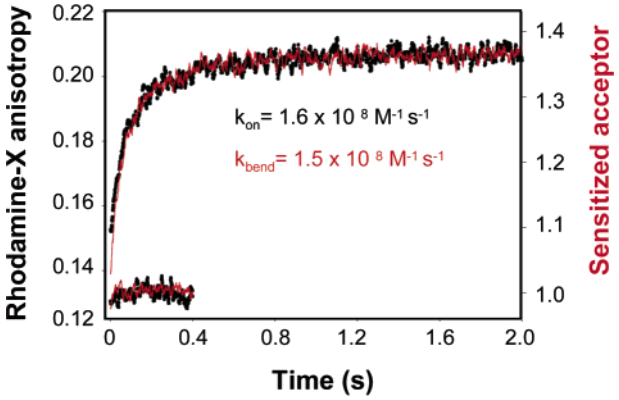


FIGURE 4: Simultaneous binding and bending kinetics. 120 nM EcoRV and 100 nM DNA were rapidly mixed in the presence of 10 mM $CaCl_2$. The binding rate is monitored by anisotropy with the substrate GCtop/RhX-GCbot (black), while bending is monitored by the sensitized acceptor with the substrate Fl-GCtop/RhX-GCbot (red). Both traces fit well to a single exponential with identical second-order rates.

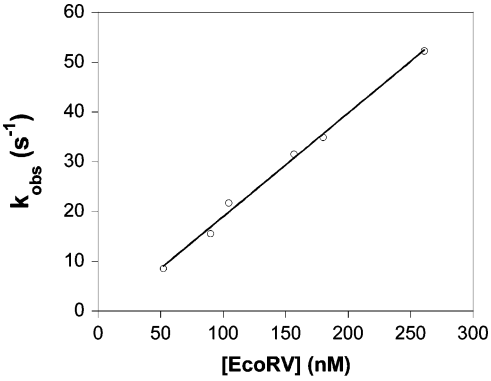


FIGURE 5: Concentration dependence of the DNA bending rate. Each point was obtained by mixing 10 nM Fl-TAtop/Rh-TAbot with a given concentration of EcoRV endonuclease by stopped flow and monitoring the sensitized acceptor emission. Data from four to eight shots were averaged to achieve an adequate signal to noise ratio and fit to a single exponential. The observed rate increases linearly with enzyme concentration, indicating that the process being monitored is second order. The intrinsic forward rate for this process (equal to the slope of the line; see Materials and Methods) is 2.1 $\times$ $10^8$ $M^{-1}$ $s^{-1}$, within experimental error of the binding rate.

provided by $Ca^{2+}$ is consistent with that observed in previous studies (*14*, *19*), although the magnitudes of the individual constants vary (see Discussion).

*Metal-Dependent Kinetics of DNA Bending.* The rate of DNA bending by EcoRV was monitored by stopped-flow FRET. Two doubly labeled specific DNA duplexes were used: (i) Fl-TAtop/Rh-TAbot and (ii) Fl-GCtop/RhX-GCbot. These substrates are each 14 base pairs in length but differ in the identity of the nucleotides flanking the GATATC site and in the identity of the acceptor fluorophore. For Fl-TAtop/Rh-TAbot FRET was measured sequentially as the decrease in donor fluorescein emission (energy transfer) and the increased emission of the acceptor (sensitized acceptor), using a commercially available stopped-flow instrument. For the Fl-GCtop/RhX-GCbot substrate a T-scheme detection system implemented in a highly sensitive home-built system (see Materials and Methods) was employed to simultaneously monitor both the energy transfer and sensitized acceptor. Identical rates were observed for both substrates as well as for either the energy transfer or sensitized acceptor measurements. This agreement provides substantial confidence that FRET is indeed the process being monitored.

Rates of DNA bending were first monitored in the presence of 10 mM $Ca^{2+}$ ions, which block DNA cleavage and thus allow isolation of the earlier binding and bending steps. When equimolar DNA and substrate are used, the observed second-order rates derived from anisotropy and FRET are nearly identical [giving rate constants of (1.45−1.6) $\times$ $10^8$ $M^{-1}$ $s^{-1}$] and may be considered effectively simultaneous within the time resolution of the experiment (roughly 5 ms) (Figure 4). Although DNA bending might be considered a first-order conformational rearrangement, the process being monitored is a combination of both binding and bending because of the necessity of starting the reaction with separate enzyme and DNA. To establish whether it is the first- or second-order process being witnessed, the concentration dependence of the observed rate with enzyme in excess of DNA was determined. If binding were much faster than bending, the observed rate of bending would have no concentration dependence; this is the case for single-turnover reactions of EcoRV, where binding is much faster than the chemical step being monitored. Instead, under conditions where enzyme is in excess over substrate, the observed rate of increase in FRET varies linearly with enzyme concentration (Figure 5). This indicates that the process being monitored is second order.

Furthermore, the bending rate must be much faster than the observed binding rate for the data to fit well to a single exponential. Using the program Kinteksim (see Materials and Methods), a fit of the fastest time course to the two-step mechanism yielded a bending rate on the order of 1000 $s^{-1}$. Though there is a great deal of error in determining this parameter, a simulated curve with the same binding rate but a bending rate of 100 $s^{-1}$ shows a lag beyond the dead time of the instrument. Thus, 100 $s^{-1}$ provides a lower limit for the bending rate of the cognate site under these conditions and shows that the actual rate is too fast to be determined using a rapid mixing device with a dead time of approximately 5−10 ms.

The complete catalytic cycle of EcoRV was observed by mixing saturating concentrations of enzyme and DNA in the presence of 10 mM $Mg^{2+}$ ions. Both fluorescence anisotropy (Figure 6) and FRET (data not shown) were used to monitor the reactions. When the reaction was initiated by adding $Mg^{2+}$ to the preincubated enzyme−DNA binary complex, a 1 s lag was observed, as reported previously in stopped-flow experiments monitoring the hyperchromicity associated with the product release step by stopped-flow absorbance (*15*). To eliminate this lag, the reaction was initiated instead by preparing the separate enzyme and DNA samples in buffer containing $Mg^{2+}$ ions. Binding and bending rates were again simultaneous and slightly higher than observed in the presence of $Ca^{2+}$ (Table 1). As the DNA is cleaved and released, the anisotropy and energy transfer substantially decrease. Figure 6 also gives an example of the concentration dependence of the association of EcoRV with DNA. Interestingly, at lower protein concentration, the bent DNA state does not become completely populated before the enzyme begins to cleave. At higher concentrations, the rate of macromolecular association is increased with respect to the rate of product release, so that the maximum anisotropy is indeed observed (Figure 6). After product release the anisotropy decreases to 0.08 (the level of single-stranded product 7-mer oligonucleotides) while the energy transfer

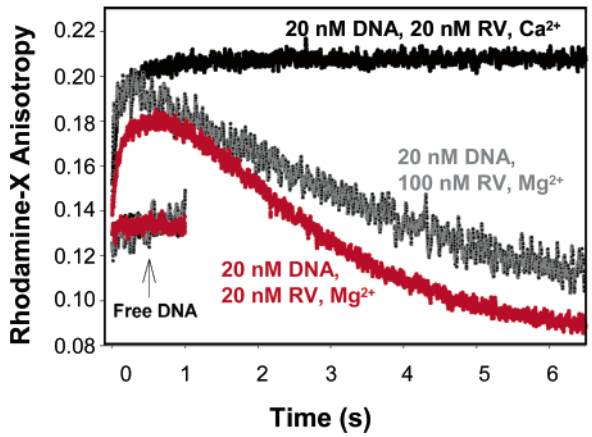


FIGURE 6: Catalytic cycle of EcoRV endonuclease monitored by fluorescence anisotropy. 20 nM GCtop/RhX-GCbot was mixed by stopped flow with 20 nM EcoRV endonuclease in the presence of 10 mM $CaCl_2$ (black), 20 nM EcoRV in the presence of 10 mM $MgCl_2$ (red), or 100 nM EcoRV in the presence of 10 mM $MgCl_2$ (gray). The anisotropy of uncomplexed DNA is also indicated. The fast increase in anisotropy is due to binding. The slower decrease corresponds to the catalytic turnover of the enzyme; once the products dissociate from the enzyme, they have a lower anisotropy than the substrate.

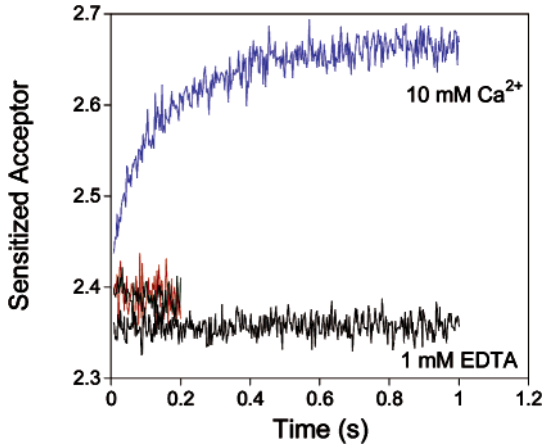


FIGURE 7: Metal dependence of DNA bending monitored by the sensitized acceptor. 80 nM EcoRV endonuclease was mixed by stopped flow with 20 nM Fl-TAtop/Rh-TAbot in the presence of 10 mM $CaCl_2$ (blue) or 1 mM EDTA (black). The fluorescence of uncomplexed DNA is also indicated (red and green, respectively). In the absence of divalent metal, there is no change in FRET efficiency.

decreases to zero (data not shown) as the cleaved DNA fragments dissociate from the protein and from each other.

Reactions were also monitored by FRET in the absence of divalent metal ions (Figure 7). However, in this case no change in the FRET signal was observed even at concentrations well above the equilibrium dissociation constant (Table 1). Thus, a stable complex of EcoRV bound to bent DNA possesssing the specific GATATC site does not form unless divalent metal ions ($Ca^{2+}$ or $Mg^{2+}$) are also present. A previous study examining DNA bending by EcoRV in solution utilized a gel mobility shift assay in which the EcoRV recognition site was located on a 418 base pair restriction fragment (*40*). While this work confirmed that the 50° DNA bending angle observed in crystal structures is closely matched in solution when divalent metals are present, no conclusions regarding bending in the absence of metals were possible. This is because of the large excess of

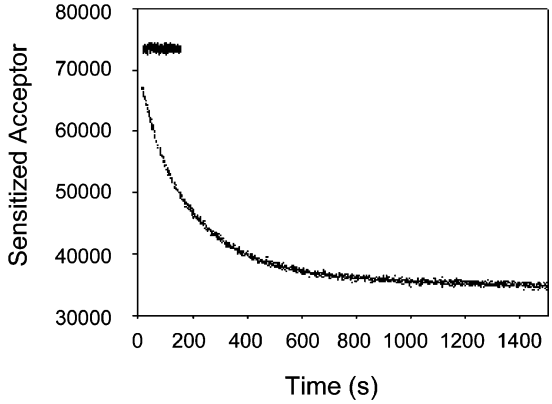


FIGURE 8: Exchange rate of metals monitored by the sensitized acceptor. 100 nM Fl-GCtop/RhX-GCbot and 110 nM EcoRV endonuclease are premixed in the presence of 10 mM $CaCl_2$. $MgCl_2$ is added to 10 mM, and FRET is monitored over time by the sensitized acceptor. As calcium exchanges with magnesium at the active site, the enzyme cleaves the DNA. After product dissociation the dyes diffuse away from each other, and the sensitized acceptor signal drops as FRET falls to zero.

nonspecific DNA together with the weak selectivity for the specific site in the absence of metal ions (*18*, *19*, *21*, *22*). Thus, in these experiments the fraction of bound enzyme actually present at the specific site is very small (*41*).

By contrast, assuming a 10 base pair interaction site as seen in cocrystal structures, the 14-mer substrates used here provide only five distinct positions at which EcoRV may bind. For $K_d$ of 14 nM (Table 1), over 90% of the DNA will be bound at 100 nM EcoRV, which represents the highest concentration used in the titration. Thus, the specific GATATC site will be 50% occupied given a 5-fold preference for this sequence in the absence of divalent metals (*19*, *21*). Indeed, the titration data (Figure 2) show that at the first titration point, where 20% of the enzyme has been added, a FRET signal from bending is already detectable. Thus, the assay would be sufficiently sensitive to detect bending even if the enzyme were randomly distributed across all five possible 10 base pair positions, corresponding to a complete absence of binding selectivity in the absence of metal ions (22). In addition, a 12-mer specific substrate possessing only three distinct EcoRV binding positions also shows no detectable bending at equivalent concentrations (data not shown), offering further support to this hypothesis. Therefore, it seems clear that DNA bending by EcoRV is less favored in the absence of metal ions. Of course, these data do not exclude the possibility that some complexes among the population are partially or fully bent in the absence of divalent metal, but they do indicate that the reversible equilibrium (Scheme 1) is shifted in the direction of unbent DNA if metals are not present to trap the scissile phosphates in the active site.

*Metal Exchange in the Enzyme−DNA Complex.* As a probe of the active site dynamics we also measured the rate of metal ion exchange at the enzyme−DNA interface. EcoRV endonuclease (110 nM) and RhX-labeled DNA (100 nM) were first equilibrated in the presence of 10 mM $CaCl_2$. Addition of $MgCl_2$ to 10 mM then resulted in a slow decrease in energy transfer (Figure 8) and in anisotropy (not shown) due to exchange of the $Mg^{2+}$ for $Ca^{2+}$ and subsequent cleavage over a 20 min time period. By contrast, the EcoRV−DNA complex requires 2 h for complete dissociation in the presence of $Ca^{2+}$ (Figure 3b). Thus, metal

exchange occurs on a much shorter time scale than does dissociation of the enzyme−DNA−$Ca^{2+}$ ternary complex, implying that the metals exchange within the intact complex. In fact, the rate constant that can be determined from this experiment may correspond to the "unbending" of the DNA ($k_{-2}$ in Scheme 1; see Materials and Methods) and may offer a further opportunity to characterize the interdependent binding and bending equilibria for wild-type and modified EcoRV−DNA complexes.

## DISCUSSION

*Synchronous DNA Binding and Bending by EcoRV Endonuclease.* Equilibrium and stopped-flow fluorescence anisotropy and FRET measurements have been used to monitor the full course of the DNA cleavage reaction by EcoRV endonuclease. Covalently modified DNA containing Fl, Rh, or RhX fluorophores attached to the 5′-ends of 14-mer duplexes were used as substrates in the experiments. Protein binding slows the tumbling of the labeled DNA resulting in an increase in anisotropy, which is monitored in the stopped-flow instrument to yield the association and dissociation rate constants. In separate experiments, FRET rates are measured as the distance between the two fluorophores decreases upon the induced-fit conformational change which includes DNA bending. These experiments show that the rates of protein binding and of DNA bending are extremely fast and nearly identical (Figures 3 and 4): the two processes occur essentially simultaneously within the roughly 5 ms time resolution of the experiments.

We also followed the rate of the $Mg^{2+}$-dependent catalytic reaction as a decrease in anisotropy after product release of the short 7-mers, which dissociate to single strands under these experimental conditions (Figure 6). Thus, the final anisotropy of the reactions is lower than that of the unbound intact 14-mer duplex substrate. The later stages of the catalytic cycle were also monitored by FRET, which decreases to zero after product release. Each method yields a first-order rate constant of 0.4 $s^{-1}$, very similar to the $Mg^{2+}$-dependent $k_{cat}$ at these conditions of pH and ionic strength. Experiments in which the EcoRV reaction cycle was monitored by changes in the intrinsic tryptophan fluorescence of the enzyme also showed that all of the initial steps in the EcoRV reaction are fast (*15*). The $k_{cat}$ of the $Mg^{2+}$-catalyzed reaction is limited by the rates of the DNA hydrolysis and product release steps, which are roughly equivalent in magnitude to each other.

The increases in either anisotropy or FRET upon association were always well fit by a single exponential to yield experimentally identical first-order observed rate constants. Thus, the binding and bending steps carried out in the presence of either $Mg^{2+}$ or $Ca^{2+}$ are not separable from each other. Given these observations, it is necessarily the case that bending occurs at a much faster rate than binding; if the rates were comparable, then the observables in the FRET experiments would exhibit more complex kinetic behavior. These data do not rule out the possibility that DNA bending is simultaneous with binding, with only one transition state. In either case, the FRET signal effectively monitors the earlier, slower binding event (*41*). However, it is important to note that this will not necessarily be the case for all EcoRV reactions. For example, the inability of EcoRV to bend DNA in the absence of metal ions (Figure 7) shows how the new FRET assay for DNA bending can provide important additional insight beyond that obtained from the previous fluorescence studies (*21*, *22*). Further, DNA bending occurs concomitantly with large-scale protein conformational changes (*7*, *8*, *20*). Thus, the FRET assay also monitors the induced-fit transition in the enzyme, making it an excellent probe for investigating which amino acids are crucial for facilitating the bending event. Alterations in the extent or rate of DNA bending can also be investigated as possible determinants of specificity against noncognate sequences.

The significant increase in FRET upon EcoRV binding in the presence of metal ions shows that DNA bending is protein-induced (Figure 1). Thus, EcoRV does not capture a fully prebent DNA conformation that is significantly populated in solution. However, there is little to no induced bending unless metal ions are present. This is in contrast to high-resolution crystal structures of the enzyme−DNA binary complex, which do reveal bent DNA even though no divalent metals are included in the crystallization mixtures (*7*, *8*). These observations may be reconciled, however, in view of the finding that binary EcoRV−DNA complexes crystallized in different crystal lattice environments show a 50% range of DNA bending angles in the absence of metal ions (*8*). It appears that the pathway of DNA bending is roughly isoenergetic, with the free energy costs of increased DNA bending compensated by improved complementarity of the protein−DNA interface in the minor groove. Thus, different protein quaternary structure states present along the pathway of bending are trapped in the distinct lattice environments. The protein movements are directly correlated with the degree of DNA bending; further, only the crystal with the most bent DNA (corresponding to a roll angle of 50° at the center TA step) is capable of sustaining catalytic activity in the lattice (*7*, *8*). Thus, the set of crystal structures may reasonably represent a part of the induced-fit transition as it occurs in solution.

Consistent with this model, we suggest that one role of metal ions is to stabilize the fully bent DNA in position to approach the transition state for cleavage. Metals appear not to be required to initiate bending, consistent with the observation that the crucial metal binding sites bridge conserved enzyme carboxylates with the DNA phosphates directly at the bending locus [a distal metal binding site located at the flanking sequences is bound only by manganese ions (*42*)]. However, if metals are absent, the unbending of the DNA to a linear conformation may occur very rapidly ($k_{-2}$ in Scheme 1; see Materials and Methods): the metal ions provide the crucial interactions to trap the bent complex. Although there may be no well-occupied distinct sites, it is likely that optimal catalysis depends on trapping of metal ions between the enzyme and DNA at the loose interface before bending is initiated. A need for trapping was suggested by rapid reaction studies, in which it was found that the hydrolysis rate is slower when $Mg^{2+}$ ions are mixed with the preformed binary EcoRV−DNA complex, as compared with reactions in which $Mg^{2+}$ was added to the enzyme and DNA prior to mixing (*15*). The very slow rate by which $Mg^{2+}$ is exchanged for $Ca^{2+}$ (Figure 8) also demonstrates a need for at least partial disruption of the enzyme−DNA interface for metals to access the active site. This exchange is somewhat faster, however, than the rate of DNA dissociation from the EcoRV−DNA−$Ca^{2+}$ complex (Figure 3b). Possibly, the rate of metal exchange represents the unbending of the DNA to form a transient complex in which the active

site is accessible.

*Thermodynamics and Kinetics of Binding by Equilibrium and Stopped-Flow Fluorescence.* The stopped-flow fluorescence methods described here may be used to derive equilibrium binding constants, by the ratio of $k_{off}/k_{on}$, across a wide range of affinities. For EcoRV $K_d$ values in the presence and absence of metal ions determined by this approach differ by nearly 4 orders of magnitude, from roughly $10^{-8}$ to $10^{-12}$ M. For even weaker binding, it is possible that $k_{on}$ may be difficult to obtain in this way, because increasingly high concentrations of enzyme and DNA must be used to measure the observed pseudo-first-order rate constants. However, in this weak-binding regime, it will be possible to measure both the equilibrium constant ($K_d$) and $k_{off}$ and thus to calculate $k_{on} = k_{off}/K_d$. Together, equilibrium and stopped-flow fluorescence are thus uniquely suited to evaluate both the thermodynamic and kinetic parameters associated with any binding event. This approach should be straightforward to adapt for other restriction endonucleases, which are generally much less well studied from a rigorous enzymology standpoint. Recently, steady-state fluorescence utilizing a substrate competition approach has also been successful in measuring the very tight DNA binding affinity characteristic of metal-dependent binding by restriction enzymes (*52*).

Attempts to use competition experiments to estimate the very tight physiologically relevant metal-dependent binding affinities by equilibrium fluorescence have not been successful (*21*). Instead, gel shift and filter binding approaches have been more commonly used to address this question (*14*, *18*, *19*). Unfortunately, both of these techniques introduce potential artifacts owing to interaction of the macromolecules with the physical matrix, are highly sensitive to small differences in experimental design, and require very substantial efforts to acquire the data in a well-controlled fashion. Work with a 381 base pair restriction fragment carrying one specific GATATC site showed that $Ca^{2+}$ stimulated a decrease in $K_d$ from 0.9 $\mu$M to 0.2 nM, an improvement in affinity of 4500-fold (*13*, *14*). This closely matches the 3800-fold stimulation measured in this study using short oligonucleotide duplex substrates. A 700-fold improvement in affinity was estimated in a different study using similar short duplexes (*18*), although values of $K_d$ were not determined. In the only previous attempt to rigorously measure the $Ca^{2+}$-dependent affinity toward short duplexes, a value of $1.2 \times 10^{-13}$ M was reported on the basis of gel shift data, some 30-fold tighter than the value of $3.7 \times 10^{-12}$ M determined here (*19*, *25*). Part of the discrepancy may arise from differences in flanking sequences and from the presence of the fluorescent probes. However, these effects are likely not to be large, because similar measurements performed on base analogue substrates in the $10^{-9}-10^{-11}$ M range gave smaller differences (as little as 3-fold; data not shown). Thus, the extremely tight $K_d$ we reported in the gel shift study for binding to the wild-type site is likely a misestimate arising from artifactual interactions with the gel matrix (*25*); this problem appears more acute for the tightest binding substrates.

The $K_d$ of 14 nM for specific site binding of short duplex substrates in the absence of metal ions is also some 10-fold higher than values reported by gel shift or filter binding studies under very similar conditions of pH and ionic strength (*18*, *19*). However, it is somewhat lower than some measurements made by equilibrium fluorescence anisotropy on this class of substrates, which range from 18 to 90 nM (*21*, *22*). Perhaps significantly, the previous estimate of 18 nM which most closely agrees with that reported here was achieved using a very sensitive hexachlorofluorescein probe (*21*). The weaker dansyl and eosin fluorophores used in the other study (*22*) may have contributed to the higher estimates; alternatively, the discrepancies might be partially accounted for by differences in the flanking sequences.

*Suitability of $Ca^{2+}$ as an Analogue of $Mg^{2+}$.* Previously, it has been suggested that $Ca^{2+}$ has the capacity to perform as a superb analogue of $Mg^{2+}$ in the binding reaction, despite its inability to support DNA cleavage. This conclusion was based on the gel shift binding analysis of a series of weakly active base analogue substrates, in which the center TA step of GATATC was replaced by UA, CI (I = inosine), or CG (*25*). $Ca^{2+}$ and $Mg^{2+}$ provided nearly identical $\Delta\Delta G^{\circ}_{bind}$ values among the base analogue sites, for which binding could be assayed in the presence of $Mg^{2+}$ owing to the very slow cleavage rates. This conclusion is strengthened by the present study. Both the $Ca^{2+}$-dependent association rate of EcoRV with DNA and the rate of DNA bending as assessed by FRET are identical in the presence of either $Mg^{2+}$ or $Ca^{2+}$ (Figure 4). Thus, the capacity of $Ca^{2+}$ to function as an analogue extends to equivalency in the kinetic steps associated with binding and induced fit and is not limited to congruence at the level of equilibrium measurements. Both $Ca^{2+}$ and $Mg^{2+}$ enhance binding affinity and specificity by shielding the otherwise present charge repulsion between the DNA phosphates and the conserved active site carboxylate groups that are required for high catalytic activity (*43*). Since $Ca^{2+}$ functions equivalently at all steps of complex formation, its inability to promote cleavage must be due solely to defects in promoting access to the near-attack conformation, in which all required catalytic elements (including the metal ions) are precisely juxtaposed adjacent to the scissile phosphates. The $pK_a$ of an inner-sphere water molecule in $Ca^{2+}$ is not greatly elevated compared with a water on $Mg^{2+}$, so the failure of $Ca^{2+}$ to promote catalysis is not primarily due to a difference in intrinsic reactivity. Instead, it appears likely that very subtle conformational adaptations in the active site that follow global bending, possibly involving small realignment of the scissile phosphates, may be impeded by the slightly larger $Ca^{2+}$ ion (*11*, *17*).

*Comparisons with Other DNA Bending Proteins.* Although EcoRV is the first restriction endonuclease for which the kinetic process of DNA distortion has been examined, synchronous DNA binding and bending also have been found in several other systems, including the chromosomal protein HMG1 (*36*), the architectural protein IHF (*34*), and the transcription factor TBP (TATA binding protein; *41*, *44*). The fact that the bending transition imposed on the DNA can be performed in a single concerted step may be the result of common design elements in these proteins, such as the presence of interspersed flexible and rigid structural domains, which allow for the concomitant protein rearrangements at relatively low free energy cost. Indeed, even the apparently more intricate rearrangement involved in "flipping" a target base completely out of the duplex stack by EcoRI DNA methylase occurs in a single rapid concerted event, together with binding (*45*). This is in contrast to many DNA polymerases that may depend on a rate-limiting conformational change for fidelity (*46*−*48*; see ref *49* for an alternative

view). In these enzymes, if the conformational change induced by noncognate substrates does not occur or is only partial, the active site is improperly assembled so that catalysis is also slowed.

In EcoRV, an important thermodynamic basis for discrimination by indirect readout arises from the bending step (*25*). TA is the most easily unstacked of any base pair step; thus, the difference in free energy cost for localized DNA bending at the center step of GATATC (compared with AT, CG, or GC) is a basis for discrimination. This thermodynamic preference, however, is also propagated into a large difference in the rate of DNA hydrolysis because the induced-fit conformational change at noncognate sites differs sufficiently to result in misalignment of catalytic groups (*25*). This phenomenon of "structural adaptation" appears to be generally the case for type II restriction enzymes (*50*). The value of the stopped-flow FRET and anisotropy in studying this crucial issue is to permit measurement of the precatalytic isomerization rate, which involves DNA bending together with the extensive protein rearrangements. Slower rates of DNA bending at noncognate sites, or for altered enzymes, may also establish specificity by effectively enhancing substrate dissociation prior to achieving the required catalytic conformation (*51*). In general, measuring the partitioning of specificity among the binding, bending, and catalytic steps should allow for a more detailed investigation of the origins of sequence selectivity in EcoRV, with possible implications to the eventual rational or semirational manipulation of target site preference.

## REFERENCES


1. Williamson, J. R. (2000) *Nat. Struct. Biol. 7*, 834−837.
2. Post, C. B., and Ray, W. J., Jr. (1995) *Biochemistry 34*, 15881−15885.
3. Jen-Jacobson, L. (1995) *Methods Enzymol. 259*, 305−344.
4. Pingoud, A., and Jeltsch, A. (2001) *Nucleic Acids Res. 29*, 3705−3727.
5. Perona, J. J. (2002) *Methods 28*, 353−364.
6. Viadiu, H., and Aggarwal, A. K. (2000) *Mol. Cell 5*, 889−895.
7. Winkler, F. K., Banner, D. W., Oefner, C., Tsernoglou, D., Brown, R. S., Heathman, S. P., Bryan, R. K., Martin, P. D., Petratos, K., and Wilson, K. S. (1993) *EMBO J. 12*, 1781−1793.
8. Horton, N. C., and Perona, J. J. (2000) *Proc. Natl. Acad. Sci. U.S.A. 97*, 5729−5734.
9. Kostrewa, D., and Winkler, F. K. (1995) *Biochemistry 34*, 683−696.
10. Horton, N. C., Newberry, K. J., and Perona, J. J. (1998) *Proc. Natl. Acad. Sci. U.S.A. 95*, 13489−13494.
11. Horton, N. C., Connolly, B. A., and Perona, J. J. (2000) *J. Am. Chem. Soc. 122*, 3314−3324.
12. Thielking, V., Selent, U., Kohler, E., Landgraf, A., Wolfes, H., Alves, J., and Pingoud, A. (1992) *Biochemistry 31*, 3727−3732.
13. Taylor, J. D., Badcoe, I. G., Clarke, A. R., and Halford, S. E. (1991) *Biochemistry 30*, 8743−8753.
14. Vipond, I. B., and Halford, S. E. (1995) *Biochemistry 34*, 1113−1119.
15. Baldwin, G. S., Vipond, I. B., and Halford, S. E. (1995) *Biochemistry 34*, 705−714.
16. Sam, M. D., and Perona, J. J. (1999) *J. Am. Chem. Soc. 121*, 1444−1447.
17. Baldwin, G. S., Sessions, R. B., Erskine, S. G., and Halford, S. E. (1999) *J. Mol. Biol. 288*, 87−104.
18. Engler, L. E., Welch, K. K., and Jen-Jacobson, L. (1997) *J. Mol. Biol. 269*, 82−101.
19. Martin, A. M., Horton, N. C., Lusetti, S., Reich, N. O., and Perona, J. J. (1999) *Biochemistry 38*, 8430−8439.
20. Perona, J. J., and Martin, A. M. (1997) *J. Mol. Biol. 273*, 207−225.
21. Reid, S. L., Parry, D., Liu, H.-H., and Connolly, B. A. (2001) *Biochemistry 40*, 2484−2494.
22. Erskine, S. G., and Halford, S. E. (1998) *J. Mol. Biol. 275*, 759−772.
23. Vipond, I. B., and Halford, S. E. (1996) *Biochemistry 35*, 1701−1711.
24. Vermote, C. L., Vipond, I. B., and Halford, S. E. (1992) *Biochemistry 31*, 6089−6097.
25. Martin, A. M., Sam, M. D., Reich, N. O., and Perona, J. J. (1999) *Nat. Struct. Biol. 6*, 269−277.
26. Clegg, R. M., Murchie, A. I. H., Zechel A., Carlberg, C., Diekmann, S. and Lilley, D. M. J. (1992) *Biochemistry 31*, 4846−4856.
27. Bloom, L. B., Otto, M. R., Beechem, J. M., and Goodman, M. F. (1993) *Biochemistry 32*, 11247−11258.
28. Kozlov, A. G., and Lohman, T. M. (2002) *Biochemistry 41*, 6032−6044.
29. Barshop, B. A., Wrenn, R. F., and Frieden, C. (1983) *Anal. Biochem. 130*, 134−145.
30. Zimmerlie, C. T., and Frieden, C. (1989) *Biochem. J. 258*, 381−387.
31. Anderson, K. S., Sikorski, J. A., and Johnson, K. A. (1988) *Biochemistry 27*, 7395−7406.
32. Wu, P., and Brand, L. (1994) *Anal. Biochem. 218*, 1−13.
33. Lavery, R., and Sklenar, H. (1989) *J. Biomol. Struct. Dyn. 6*, 655−667.
34. Lorenz, M., Hillisch, A., Goodman, S. D., and Diekmann, S. (1999) *Nucleic Acids Res. 27*, 2619−4625.
35. Vámosi, G., Gohlke, C., and Clegg, R. M. (1996) *Biophys. J. 71*, 972−994.
36. Jamieson, E. R., Jacobson, M. P., Barnes, C. M., Chow, C. S., and Lippard, S. J. (1999) *J. Biol. Chem. 274*, 12346−12354.
37. Parkhurst, K. M., Brenowitz, M., and Parkhurst, L. J. (1996) *Biochemistry 35*, 7459−7465.
38. Ozaki, J., Iwase, N., Sawai, H., Kodama, T., and Kyogoku, Y. (1997) *Biochem. Biophys. Res. Commun. 231*, 553−556.
39. Nazarenko, I., Pires, R., Lowe, B., Obaidy, M., and Rashtchian, A. (2002) *Nucleic Acids Res. 30*, 2089−2095.
40. Stover, T., Kohler, E., Fagin, U., Wende, W., Wolfes, H., and Pingoud, A. (1993) *J. Biol. Chem. 268*, 8645−8650.
41. Parkhurst, K. M., Brenowitz, M., and Parkhurst, L. J. (1996) *Biochemistry 35*, 7459−7465.
42. Sam, M. D., Horton, N. C., Nissan, T. A., and Perona, J. J. (2001) *J. Mol. Biol. 306*, 851−861.
43. Selent, U., Reuter, T., Keohler, E., Liedtke, M., Thielking, V., Alves, J., Oelgeschleager, T., Wolfes, H., Peters, F., and Pingoud, A. (1992) *Biochemistry 31*, 4808−4815.
44. Perez-Howard, G. M., Weil, P. A., and Beechem, J. M. (1995) *Biochemistry 34*, 8005−8017.
45. Allan, B. W., Reich, N. O., and Beechem, J. (1999) *Biochemistry 38*, 5308−5314.
46. Hsieh, J.-C., Zinnen, S., and Modrich, P. (1993) *J. Biol. Chem. 268*, 24607−24613.
47. Zhong, X., Patel, S. S., Werneburg, B. G., and Tsai, M.-D. (1997) *Biochemistry 36*, 11891−11900.
48. Johnson, K. A. (1993) *Annu. Rev. Biochem 62*, 685−713.
49. Showalter, A. K., and Tsai, M.-D. (2002) *Biochemistry 41*, 10571−10576.
50. Jen-Jacobson, L. (1997) *Biopolymers 44*, 153−180.
51. Allan, B. W., Garcia, R., Maegley, K., Mort, J., Wong, D., Lindstrom, W., Beechem, J. M., and Reich, N. O. (1999) *J. Biol. Chem. 274*, 19269−19275.
52. Parry, D., Moon, S. A., Liu, H.-H., Heslop, P., and Connolly, B. A. (2003) *J. Mol. Biol. 331*, 1005−1016.


BI035520W